Intersecting Fluvial and Pluvial Inundation Estimates with Sociodemographic Vulnerability to Quantify Household Risk in Urban Areas

M. Preisser[1,2], P. Passalacqua[1], R.P. Bixler[2], and J. Hofmann[3]

[1]Environmental and Water Resources Engineering, University of Texas at Austin, Austin, Texas, USA.
[2]LBJ School of Public Affairs, University of Texas at Austin, Austin, Texas, USA.
[3]Institute of Hydraulic Eng. & Water Resources Management, RWTH Aachen University, Germany.

Key Points:

- We intersect inland urban compound inundation mapping and social vulnerability to estimate residential flood risk in near-real time.
- Pluvial flooding that occurs in topographic and anthropogenic depressions in the landscape increases urban flood extents.
- Aggregating flood hazard estimates to cartographic boundaries can misrepresent risk by masking its inequitable distribution.

Corresponding author: Dr. Paola Passalacqua, `paola@austin.utexas.edu`

Abstract

Methods to estimate compound flooding at the household level are largely nonexistent outside of complex computational models. The exclusion of topographic depressions, and therefore pluvial flooding, from leading flood hazard maps is also underestimating potential exposure. Furthermore, national level exploratory analyses have yet to capture local variability in exposure and social vulnerability, which is necessary for local stakeholders to identify the inequitable distribution of flood risks. Using high resolution elevation data to approximate event specific inundation from both pluvial and fluvial sources, in conjunction with a localized social vulnerability index, we created a methodology to estimate flood risk at the household level. Our analysis uses the 2015 Memorial Day Flood in Austin, Texas as a case study and proof of concept of our estimation methodology. We show that the inclusion of pluvial flood sources increases inundation extents, with 37% of the Census Block Groups in the study area experiencing flooding from only pluvial sources. Furthermore, averaging flood depths, and therefore exposure estimates, to geographical and cartographic boundaries (e.g., Census Block Groups), masks household variability, with 80% of the Census Block Groups in the study area having a coefficient of variation around the mean flood depth exceeding 100%. Comparing our pluvial flooding estimates to a 2D hydrodynamic physical-based model, we classified household exposure accurately for 92% of the parcels. Our methodology can be used as a tool to estimate the impacts of inland compound flooding on household risk in order to provide a first estimate of storm specific risk.

Plain Language Summary

There is rising concern in numerous fields in quantifying the inequitable distribution of human risk to floods. Flooding risk can be defined as the intersection of an individual's exposure to a flood event and their social vulnerability. The co-occurrence of fluvial (river) and pluvial (surface) flooding is largely excluded from the leading flood hazard mapping services, therefore flood exposure is often underestimated. In addition, many exploratory studies of flood exposure and social vulnerability rely on low-resolution elevation data and aggregate risk estimates within geographic and cartographic boundaries, therefore masking small-scale variabilities. Using high-resolution elevation data and a localized social vulnerability index, we developed a method to estimate risk at the household level in near-real time, using the 2015 Memorial Day Flood in Austin, Texas (USA) as a case study.

1 Introduction

Flooding is the natural hazard with the greatest economic and societal impacts in the United States, and these impacts are becoming more severe over time (National Academies of Sciences Engineering and Medicine, 2019). In conjunction, as of 2019, over 80% of the United States population lives in urban areas. The total US population at risk of serious flooding ranges from 13 to 41 million people, depending on the flood model, with high amounts of uncertainty and underestimation in urban centers (Wing et al., 2018). Urban flood waters come from three main sources: fluvial sources, as rivers and streams exceed their banks, pluvial sources from overland runoff, and coastal sources such as storm surges, tides, and waves. While coastal and fluvial threats are reported in leading flood hazard maps such as those produced by the Federal Emergency Management Agency (FEMA), these maps lack information regarding the threat of pluvial flood waters. Despite this, end users, such as emergency responders and city planners, frequently request maps including pluvial flood hazards and ponded water depths/extents (Luke et al., 2018). It is of specific concern to numerous government agencies that pluvial flooding be included in flood warning, mapping, and risk management efforts, including the specific identification of topographic depressions that allow for the ponding of water (Falconer et al.,

2009). The goal of this paper is to produce a single measure of flood hazard risk at the parcel level, using a near-real time inland compounding flooding estimate and a localized social vulnerability index.

Depressions are topographic areas that do not drain and have no outward flow when only partially filled with water. These areas have a negative relative relief or a lower elevation in reference to their surrounding boundaries (Lewin & Ashworth, 2014). Depressions also form in areas that have little to no change in elevation producing no lateral flow (Le & Kumar, 2014). Depressions are not limited to single low points in elevation, rather they can have complex connected structures. Depending on residual water level, height, soil moisture, and upstream drainage, these depressions can fill, spill, and merge into adjacent low points. Specifically, depressions begin to fill when runoff water exceeds evaporation and infiltration capacity until the depression storage threshold is reached and overland flow begins (Hu et al., 2020). Depressions are formed through a variety of processes along different sections of alluvial plains, ranging from centimeters to kilometers in scale, and play a critical role in sediment deposition and water accumulation, suggesting the necessity to include such features in flood management and forecasting (Syvitski et al., 2012). A depression's properties vary over different landscapes, and therefore can significantly influence numerous hydrological processes including delaying the initial time of runoff yield, total volume of outflow, increasing soil surface roughness, and reducing overland flow velocity (Hu et al., 2020).

Compound flooding broadly refers to the co-occurrence of flooding from rainfall (pluvial and fluvial flooding) and coastal sources (Wahl et al., 2015; Muthusamy et al., 2019). However, pluvial and fluvial flooding can have their own compounding effects in land locked regions, occurring through one of two possible mechanisms: compounding in both time and space or compounding in only time (Wahl et al., 2015). For the former, pluvial and fluvial flooding occur at the same location at the same time. This mechanism occurs in depressions directly adjacent to and within fluvial floodplains, which have the potential to be impacted from both fluvial and pluvial floodwaters. For the latter, compound effects are only in time, meaning that pluvial and fluvial flooding occur at the same time over a broader region. When pluvial and fluvial flooding occur simultaneously across a city in multiple locations, emergency services have to be divided, thus further constraining access to resources. Regardless of the type of compound flood occurring, all floodwaters will contribute to the overall watershed discharge. Topographic depressions can be integrated into urban flood planning to identify risk associated with the compounding effects of fluvial and pluvial flooding.

Areas most at risk during flooding events can be identified by overlaying flood exposure maps with social or sociodemographic vulnerability maps (Rufat et al., 2015). This process is useful in order to discern emergency management plans and identify potential environmental justice concerns (Chakraborty et al., 2014). Kaźmierczak and Cavan (2011) identified four characteristics of people and their households that influence vulnerability (in the context of flooding): access to information, ability to prepare for flooding, ability to respond to flooding, and ability to recover. These factors are influenced by the individual and household's social and demographic characteristics. Survey data measuring household flood vulnerability (the four previous characteristics) can be targeted to specific flooding scenarios or events and can be insightful to local and regional planners. However, low survey response rates, inadequate sampling methods, and time between surveys can make these surveys obsolete after a few years when considering the long-term effects and trends of urban flooding (Collins et al., 2019). Therefore, social vulnerability indices (SVIs) based on more commonly measured metrics (e.g., household income, household size, age, race, ethnicity, housing type, access to healthcare, access to transportation) are utilized as a proxy in general vulnerability applications.

SVIs measure both the sensitivity of a population to natural hazards and its ability to respond to and recover from the impacts of a hazard. SVIs often rely on national

level survey data, such as the US Census Bureau's American Community Survey (ACS). ACS data have numerous strengths when compared to primary survey methods because methods/data are standardized across geographies, are available for all geographies, and are free to use. Survey data are often aggregated at coarser resolutions than those of flood models (e.g., Census Block Groups, Tracts, Zip Codes, Counties, etc.). This operation is done for a variety of reasons including protecting individual privacy and for strategic statistical sampling purposes to reduce the necessary resources (time and money). However, the use of such boundaries does not provide a level of precision sufficient enough for the identification of significant disparities in flood exposure, thus limiting a community's ability to provide emergency services adequately to those most in need (Nelson et al., 2015).

Our study acts as a proof of concept for a new workflow to forecast storm specific flood exposure and risk in urban environments, using the 2015 Memorial Day Flood in Austin, Texas as a case study. We quantify fluvial and pluvial flood exposure in urban areas using high resolution digital elevation models (DEMs), identifying if there is a significant difference in flood exposure estimates when considering only fluvial and both fluvial/pluvial sources. Furthermore, we combine residential flood exposure with relative sociodemographic vulnerability scores to estimate risk at the parcel level. In the context of Census Block Groups, these results highlight how aggregating flood exposure and risk estimates to cartographic boundaries fails to capture important variability at local scales. The inequitable distribution of flood risk burdens on different communities is more accurately described when examining exposure and vulnerability values at the parcel level. This information can help local officials to discern the extent to which possible environmental justice concerns exist within the study region.

This paper is organized as follows: first we provide background information (Section 2) on terrain, social vulnerability, and risk, cover the characteristics of our study area and data sources (Section 3), and then explain our workflow and methodology (Section 4). We present results (Section 5) for the 2015 Memorial Day Flood and discuss them (Section 6). Finally, we state the conclusions of this work and opportunities for future research (Section 7).

2 Background

2.1 Fluvial Inundation Mapping

Future fluvial flood risk is one of the most commonly researched impacts of climate change (Arnell & Gosling, 2016; Winsemius et al., 2016; Alfieri et al., 2017). Fluvial flooding is researched and studied at all spatial resolutions from global models to individual streams, and approaches to estimate fluvial flooding can be categorized as empirical methods (observation based), hydrodynamic models (mathematical and physics based), and simplified conceptual models (non-physics based), each with their own advantages and disadvantages (Teng et al., 2017). This analysis uses an existing terrain based simplified conceptual model to estimate fluvial flooding (GeoFlood) because it has been shown to be able to capture the general inundation patterns of flooding events as well as have a significant potential in guiding real-time flood disaster preparedness and response (Zheng et al., 2018). Since the use of high resolution terrain data in flood inundation has been covered in previous work, we refer the reader to the GeoFlood publication (Zheng et al., 2018) and references therein. Since the novelty of our study relies on the integration of pluvial flooding and vulnerability into this approach, we provide more background on these specific components.

2.2 Modeling Surface Water in Depressions

Prior to the recent increase in availability of lidar data, depressions in coarser resolution DEMs (+30 meters) were seen as errors in the data collection process and were subsequently filled in or removed to ensure that water flowed continuously downstream (Li et al., 2011; Callaghan & Wickert, 2019). Flood-fill, breaching, carving, and combination algorithms modify the DEM by raising and/or lowering cells to create a depressionless surface (Jenson & Domingue, 1988; Martz & Garbrecht, 1999; Soille et al., 2003; Lindsay & Creed, 2005). Alternatives to modifying elevation data also exist through the use of a least-cost drainage path algorithm that is able to pass through depressions (Metz et al., 2011). Regardless of the method used, these algorithms produce hydrologically connected elevation surfaces by ignoring or removing depressions in the DEM and discounting their significant hydrologic impact (Callaghan & Wickert, 2019). With lidar technology and the availability of high resolution DEMs (1-meter and finer), topographic analyses can incorporate existing depressions, both naturally occurring and from anthropogenic sources. Depressions can be identified through a variety of methods utilizing remote sensing and automation techniques. Identification methods typically begin by comparing a filled and unfilled DEM (i.e., a depressionless DEM and the original DEM) to identify areas that are different. From here, methodologies vary slightly in their ability to eliminate noise in data and to represent the complex nested hierarchy of depressions. Some methods utilize elevation profiles (Wu et al., 2016), simplified hierarchical trees (Wu & Lane, 2016), or filtering based on threshold variables for surface area, depth, or volume (de Carvalho Júnior et al., 2013). Numerous methods exist to model how surface water moves through complex depressions with possible applications to micro- and macro-topographical features. Examples include the puddle-to-puddle (P2P) model, which routes a gridded rainfall depth, and the Fill-Spill-Merge algorithm, which routes a gridded runoff depth (Chu et al., 2013; Barnes et al., 2019b). Surface water storage volumes and ponded water extents are outputs of these two models.

P2P delineation was first discussed in reference to microtopographic depressions, or depressions at the millimeter scale (Chu et al., 2013). P2P exists as a full physically based overland flow model, coupled with infiltration and unsaturated flow models that can handle spatiotemporally varying rainfall conditions (both single and multiple rainfall events). This model introduced the idea of cell-to-cell, and subsequently puddle-to-puddle routing of water and identifies the importance and necessity of incorporating topographic depressions in overland flow modeling, specifically as the spatial resolution of elevation data increases. However, given the computationally expensive nature of P2P and other similar overland flow models that utilize cell-by-cell algorithms, near-real time analyses need a more efficient approach that is able to be broadly applied across a large landscape (e.g., an urban watershed). The algorithm chosen for this study is Fill-Spill-Merge, a mass-conserving approach that uses a network based algorithm (Barnes et al., 2019a, 2019b).

Fill-Spill-Merge utilizes a depression hierarchy and represents the topologic and topographic complexity of depressions across a landscape as a network. Sub-depressions can merge to form meta-depressions, and a depression hierarchy tree can selectively fill and breach depressions based on the volume of water in them. The Fill-Spill-Merge workflow can be described in four steps: First, Fill-Spill-Merge calculates the depression hierarchy, flow directions, and label matrix needed to route water over the landscape. Second, water is routed to its lowest downslope pit, assigning it to the appropriate leaf in the hierarchy. Third, moving through each leaf, water that overflows from a depression is redistributed to siblings and parents within the hierarchy. Fourth, the algorithm determines the final depths based on if the depression is completely filled, partially filled, or empty.

The implementation of the depression hierarchy and routing process between leaves, siblings, and parents makes this algorithm independent of the runoff depth, therefore dras-

218 tically increasing its computational speed at higher runoff values when compared to cell-
219 by-cell algorithms by a factor ranging between 2,000 – 63,000 (Barnes et al., 2019b). Fill-
220 Spill-Merge's ability to efficiently route water over a complex landscape is therefore ideal
221 in determining the extent and depths of pluvial flood waters. While Fill-Spill-Merge was
222 originally tested on coarse resolution DEMs (ranging between 15-meter and 120-meter
223 cell size), this analysis looks to apply Fill-Spill-Merge on a higher resolution DEM (1-
224 meter resolution).

2.3 Risk as a Function of Vulnerability and Exposure

226 This analysis' focus is on the intersection of social vulnerability and urban inun-
227 dation mapping. It is therefore important to clarify the differences and relationships be-
228 tween principal ideas, such as adaptive capacity, sensitivity, exposure, hazard, vulner-
229 ability, social vulnerability, and risk, within the social sciences and engineering fields. In
230 the context of social sciences, adaptive capacity is the degree to which an individual or
231 community is able to respond to or cope with change quickly and easily. Exposure and
232 sensitivity characteristics, which are made up of such variables including social, polit-
233 ical, cultural, and economic conditions, influence and constrain adaptive capacity (Smit
234 & Wandel, 2006). Understanding the interconnected relationships among exposure, sen-
235 sitivity, and adaptive capacity is important to estimate the degree to which stakehold-
236 ers can mitigate environmental hazards (Smit & Wandel, 2006). Social vulnerability, as
237 seen by social scientists, serves as a proxy for a community's sensitivity and adaptive ca-
238 pacity. SVIs are therefore built on sociodemographic data and can incorporate multi-
239 hazard exposure estimates for a final metric that represents a community's resiliency (Smit
240 & Wandel, 2006).

241 The original calculation and most frequently cited tool for estimating social vul-
242 nerability within the United States is the Social Vulnerability Index SoVI® (Cutter et
243 al., 2003). SoVI® synthesizes 42 socioeconomic and built environment variables to quan-
244 tify the social vulnerability to environmental hazards and generate a comparative met-
245 ric that facilitates the examination of the differences between U.S. counties (Cutter et
246 al., 2003). Since its inception, it has been revised numerous times (SoVI® 2010-2014)
247 and reduced to 29 socioeconomic variables. Since then, numerous social vulnerability in-
248 dices, both global and regional, including those created by the United Nations Devel-
249 opment Program and the Center for Disease Control (UNDP, 2010; Flanagan et al., 2011)
250 have been developed and widely used. Different constructs and variations of SVIs have
251 different levels of predicative power, and therefore require fine tuning for each specific
252 use (Rufat et al., 2019). Both SoVI® and the CDC's SVI, two of the most commonly
253 cited SVI's that specifically focus on the US, estimate social vulnerability at the county
254 level. Due to the vulnerability heterogeneity that exists within counties, variance can go
255 undetected which can adversely affect at risk populations. With the onset of sociode-
256 mographic data available at higher than county resolutions, similar methodologies ap-
257 plied by Cutter et al. (2013) can be applied for higher resolution boundaries.

258 In the context of engineering, environmental risk represents the possibility of an
259 event adversely affecting the normal function of a community or society (Cardona et al.,
260 2012). In its simplest terms, risk is the product of a hazard and its consequences, with
261 a hazard being any natural event including the probability of its occurrence. Consequences
262 are the value of items at risk and the vulnerability of such value (Kron, 2005). This def-
263 inition of risk is further explained by the Office of the United Nations Disaster Relief Or-
264 ganization (UNDRO) as "the expected losses from a particular hazard to a specified el-
265 ement at risk in a particular future time period" (Peduzzi et al., 2009). Risk is there-
266 fore the product of frequency (i.e., probability of occurrence), exposure, and vulnerabil-
267 ity variables. This analysis focuses on estimating risk from a single flood event (i.e., fre-
268 quency is equal to 1 because it did occur).

Previous attempts have been made to disaggregate social vulnerability variables to a finer scale, such as down to individual tax parcels (Nelson et al., 2015). General methodologies follow the same core concept of using dasymetric mapping techniques, which utilize ancillary datasets to divide mapped areas into new but still relevant zones, such as tax parcels. This method is commonly used with cadastral data (land use/land cover data) to divide other geographic boundaries. Nelson et al. (2015) discusses using cadastral-informed selective disaggregation logic to both extract relevant social vulnerability variables from tax parcel layers while dissolving Census Block Group variables to produce a parcel level SVI estimate. Our analysis uses dasymetric techniques to dissolve Census Block Group variables to residential parcels, but does not use a selective disaggregation logic. While geographic tax parcel data are widely available (e.g., parcel boundaries), some associated variables (e.g., housing type, property value, gross rent, etc.) are not consistently reported across counties, regions, and states. Therefore, for vulnerability uniformity purposes, this analysis extracted all social and demographic variables from the ACS report.

3 Study Area and Data Sources

Austin, Texas, considered one of the fastest growing cities in the US, has a population approaching one million residents. In conjunction with rapid urbanization to accommodate for the influx of new residents, Central Texas has seen an increase in the occurrence of 1% annual exceedance probability storms, experiencing three in a five-year window, including the 2013 Halloween Day Flood, 2015 Memorial Day Flood, and the 2018 Hill Country Flood. These events pose a risk to new residents as increased development, and subsequent expansion of impervious surfaces, increase people's potential exposure to both pluvial and fluvial flooding. Dividing Austin, Texas in the middle is the Colorado River, which is dammed by the Tom Miller Dam to the north and the Longhorn Dam to the south. There are also numerous major creeks throughout the northern and southern sections of Austin. This study focuses on the region of Austin that is north of the Colorado River containing the majority of new developments, major creeks, and population groups within Austin(Figure 1 & Table 1). Furthermore, this area encompasses a wide range of demographic groups stretching from West to East Austin, as well as encompassing the downtown and University of Texas areas. When discussing exposure, vulnerability, and risk at the parcel level, our analysis only considers residential parcels within the formally defined Austin neighborhood boundary.

We use the 2015 Memorial Day flood in our analysis, as this event is often referred to as the worst flood in recent Austin history. The data sources and tools used were deliberately chosen for their broad accessibility across the country, allowing the application of this methodology to occur across the US with little to no data availability concerns (Table 2). Stream reaches, their boundaries, streamflow discharge, and rainfall are all publicly available and provided by the USGS and NOAA. 1-meter DEMs for the contiguous United States are also broadly available through the USGS, as well as through other state and regional agencies. Parcel boundaries are well defined across the country, and while a single national source is not publicly available, most city and state agencies will provide this information for free. For example, the Texas Natural Resources Information System (TNRIS) currently has 228 of 254 counties' parcel data available for free.

The American Community Survey (ACS) 5-Year Estimates are period estimates that represent data from the previous 60 months, the largest sample size when compared to other ACS reports. For example, the 2017 data used in this analysis is an aggregation of data collected from 2013 through 2017. This large sample size is able to dampen outliers and potential errors in sociodemographic data. ACS 5-Year Estimates are available for all block groups across the US, the highest spatial resolution that Census Bureau publishes data at, and is therefore able to capture variation in the demographic makeup
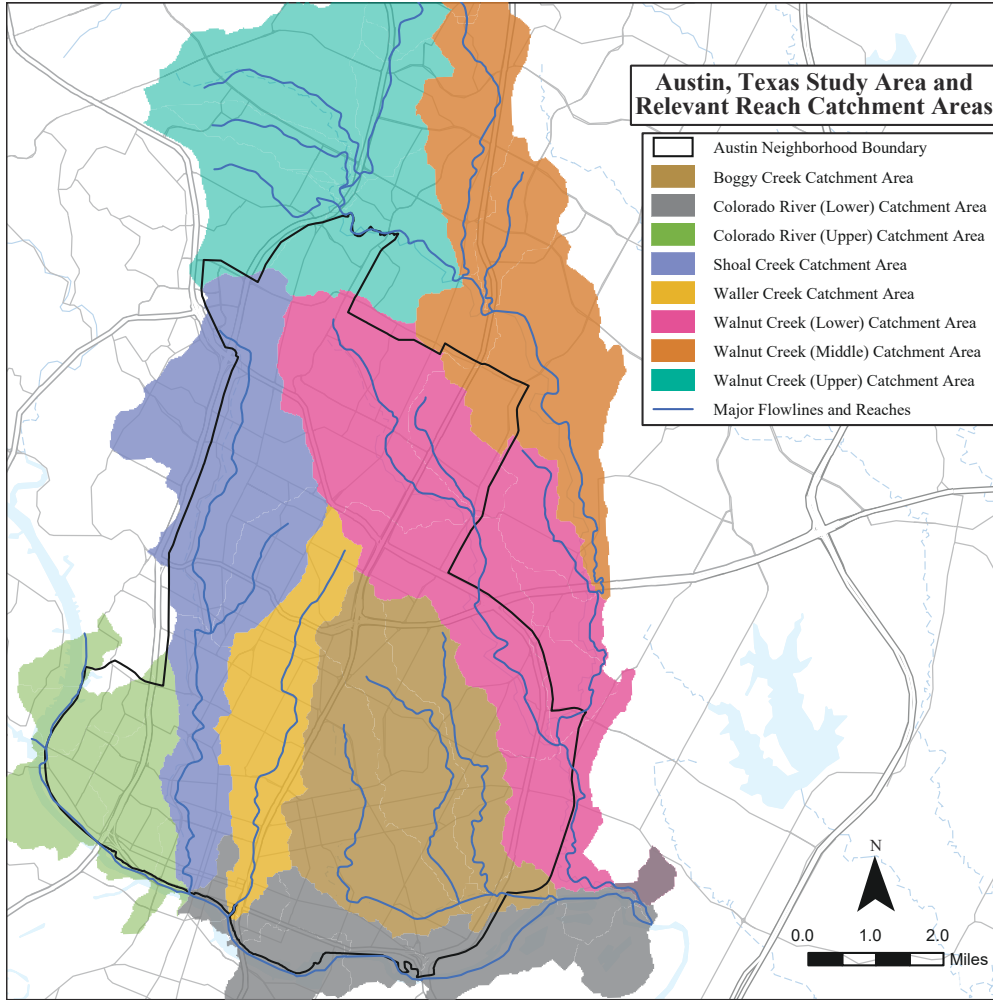
Figure 1. Austin, Texas study area boundary and relevant stream reach catchment areas.

320 of a region. Block Groups have a population ranging from 600 to 3,000 people, depend-
321 ing on if the block group is in a more rural or urban location.

322   ACS 5-Year Estimate reports at the Block Group level are not without disadvan-
323 tages. Block Groups are not perfect delineations of neighborhoods, and can unintention-
324 ally group dissimilar individuals, creating a large margin of error in some estimations.
325 ACS 5-Year Estimates are also the least current datasets available due to their 5-year
326 look back nature. This 5-year look back period also limits comparisons that can be made
327 between datasets since only a few non-overlapping datasets exist. However, compared
328 to other ACS reports and the difficulties and expenses of other survey data sources, the
329 advantages of using the ACS 5-Year Estimates reports outweighs the disadvantages pre-
330 sented. This analysis uses social and demographic data from the 2017 ACS 5-Year Es-
331 timates report, the most recently available at the time of calculation and that best cap-
332 tures the conditions relevant to the 2015 flood event.

Table 1. Austin, Texas catchment characteristics.

Catchment Name	Mean of Daily Mean Discharges ($m^3 \cdot s^{-1}$)	Instantaneous Peak Discharge[a] ($m^3 \cdot s^{-1}$)	Total Rainfall Depth[b] (cm)	USGS Stream Gauge Number
Walnut Creek (Lower)	2.49	328.5	13.2	08158600
Walnut Creek (Middle)	1.39	475.7	13.2	08158200
Walnut Creek (Upper)	1.39	475.7	13.2	08158200
Boggy Creek	0.14	37.9	13.2	08158035
Shoal Creek	0.45	311.5	13.2	08156800
Waller Creek	0.25	131.4	13.2	08157560
Colorado River (Lower)	9.97	982.6	13.2	08158000
Colorado River (Upper)	9.97	982.6	13.2	08158000

[a]Peak instantaneous discharge was used as a representation of the worst-case scenario and of the flash-flood characteristics related to the Memorial Day Flood.

[b]Total rainfall represents the total amount of precipitation that fell on Memorial Day (May 25th, 2015) over a 24-hour period. 13.2 cm of rain is approximately a 0.005 annual exceedance probability for this region (according to NOAA historical precipitation data).

Table 2.   Programming tools and data sources utilized in this methodology.

Tool/Data Name	Resolution	Source	Description and Purpose
Fill-Spill-Merge	NA	(Barnes et al., 2019b)	Utilizing a depression hierarchy, routes water through a topographic surface in order to map ponded water
GeoNet	NA	(Passalacqua et al., 2010)	Geometric framework to extract channel networks from high resolution topographic information
GeoFlood	NA	(Zheng et al., 2018)	Builds on GeoNet in order to create inundation maps based on streamflow data and the HAND method
Parcel Boundaries	NA	TNRIS	Parcel boundaries with land use classification. Only residential parcels were considered
Elevation (DEM)	1-meter	TNRIS	Topographic extent of the study region
Stream Reaches	NHD-MR	USGS	USGS maintained stream reach shapefile for the study region
Stream Reach Boundaries	NHD-MR	USGS	USGS maintained stream catchment area shapefile for the study region
Streamflow Discharge	NA	USGS	The peak instantaneous discharge during the flooding event for each catchment area was used for fluvial flooding inundation estimation
Rainfall	NA	NOAA	24-hour rainfall total in inches for the study region
American Community Survey: 2013-17 5 Year Estimates	Block Group	US Census Bureau	ACS 5-year socio-economic data by block group
Census Block Group Boundaries	NA	US Census Bureau	Shapefile acquired from Census database. There are 177 block groups in the study area

4 Methodology and Workflow

The following subsections detail the methodology and workflow for calculating flood exposure, sociodemographic vulnerability, and flood risk at the parcel level (Figure 2).
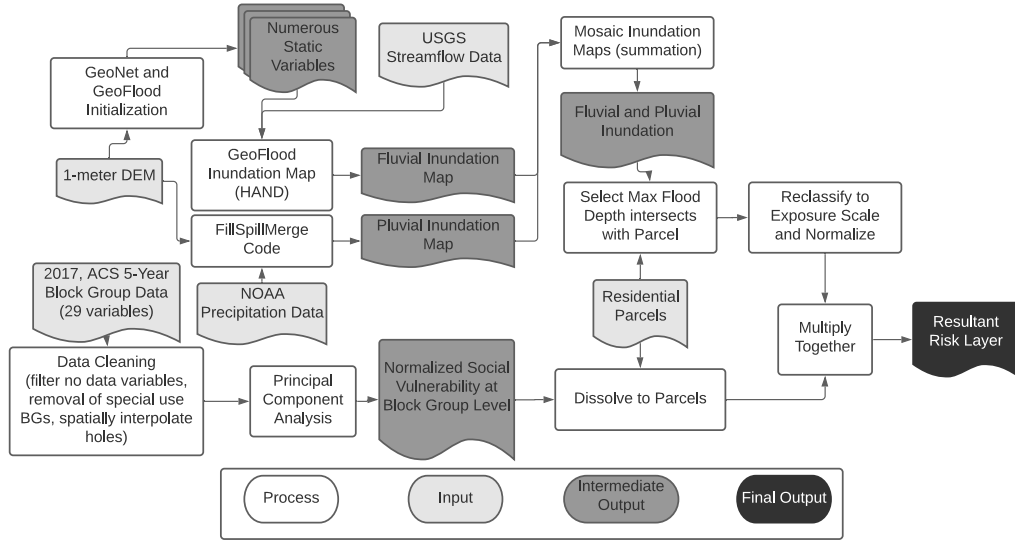
Figure 2. Complete workflow of our approach including fluvial/pluvial inundation estimation and SVI calculation.

4.1 Flood exposure at the parcel level

The 1-meter DEM was first processed using the GeoNet workflow (Passalacqua et al., 2010; Sangireddy et al., 2016). GeoNet extracts channel networks from high resolution topography data through the application of nonlinear filtering and the identification of geodesic paths as curves of minimum cost. GeoNet uses a Perona-Malik nonlinear smoothing image filter (set to 50 iterations) to remove observation noise and irregularities within the DEM. This non-linear filter uses gradient information to define the diffusion coefficient in order to preferentially smooth regions outside and within the channel, rather than across its boundary, in order to maintain clear channel boundaries. GeoNet is able to calculate both a geometric and Laplacian curvature based on the desired use. We chose to use the geometric curvature in order to normalize across the entire study region (as compared to the Laplacian calculation which is more selective). GeoNet uses this information, along with flow accumulation, flow direction, and slope in a cost function representing travel between two points to determine the geodesic curve from the channel head to the basin outlet. Terrain and hydrological outputs from GeoNet are integrated within GeoFlood, which creates, through the application of the Height Above Nearest Drainage (HAND) method, an inundation map (extent and depths of flood waters) along the delineated stream channels for a given input flow rate (Nobre et al., 2011; Zheng et al., 2018). To summarize, given a known centerline water depth, h, at a river segment, the HAND raster is used to produce a water depth grid of the inundated area, $F(h)$, within the local catchment draining to that segment. The water depth, d, at any location, i, is therefore

$$d_i = \begin{cases} h - hand_i & if \ \ hand_i \leq h \ \ (flooded, i \in F(h)) \\ 0 & if \ \ hand_i > h \ \ (not flooded, i \notin F(h)) \end{cases} \tag{1}$$

The Fill-Spill-Merge algorithm determines the pluvial inundation depths and extents using a uniform runoff depth across the study region. The storm being analyzed had numerous days of heavy rain leading up to the peak flood. This condition led to saturated soils for the majority of downtown Austin, justifying using rainfall depth as an equivalent for runoff depth. The rainfall depth is routed through the depression hierarchy to its lowest down stream point before being redistributed to nodes with enough volume to contain the volume of rainwater, with the excess being sent to the "ocean" (Barnes et al., 2019b). Fill-Spill-Merge requires an input elevation that is equal to the lowest elevation across the DEM which serves as the "ocean", or the super-sink of the network that all water not remaining in a depression drains to. To accommodate this, we added an artificial elevation along the entire perimeter of the DEM that was set to 0-feet. To summarize, given a known volume of water in a depression, V_w, and the raster cells within that depression, $c_i = c_1, ...,c_N$, the water level in the depression, Z_w, is therefore

$$Z_w = \frac{1}{N} * (V_w + \sum_{n=1}^{N} Z_i) \tag{2}$$

with each cell in the depression having a water elevation equal to the computed Z_w. For a more detailed explanation of this algorithm, we refer the reader to the Fill-Spill-Merge publication (Barnes et al., 2019b) and references therein.

The inundation extents produced by GeoFlood and Fill-Spill-Merge, eq. [1] and [2], are merged to estimate the compound exposure. Merging the worst-case exposure to fluvial and pluvial flooding will create an inundation layer that is the worst-case overall. The worst-case exposure to fluvial flooding occurs during the absolute maximum of stream flow, and pluvial flooding after the total cumulative rainfall depth. The worst-case exposure scenario does not depend on the temporal distribution of flood waters, and therefore this analysis only requires the peak instantaneous discharge, which may occur at varying times for each stream reach, and the total accumulated rainfall depth. Using raster math functions, the fluvial and pluvial inundation estimates are summed. This summation specifically highlights areas that will experience both fluvial and pluvial flooding.

Residential parcel exposure to flooding was determined by overlaying the inundation and parcel layers and extracting the highest flood depth that intersects each parcel. Numerous factors affect an individual's flood exposure, including but not limited to the flood duration, depth of water, velocity of storm water, and water quality (Middelmann-Fernandes, 2010). Therefore, there is uncertainty regarding the direct correlation between flood depth and flood damage (Freni et al., 2010). Regardless, flood depth-damage relations remain one of the leading methodologies for flood exposure estimation in numerous leading models (de Moel & Aerts, 2011). For this study, flood depth remains the quickest and easiest proxy for exposure to flooding.

Adapting methods from other flood communication research, flood depths are reclassified and binned to a more easily understandable scale that relates water depth to various heights along the average person's body (Calianno et al., 2013; Ahmed, Khan, et al., 2018; Ahmed, Moors, et al., 2018). This approach avoids the over/under inflation of other relative exposure results. For example, if all flood depths were min-max normalized, a small regional flood would appear to have a similar exposure to a large regional flood. Therefore, a household's exposure refers to the reclassified maximum inundation depth, d_{max}, at that parcel (Eq. [3]). The reclassified flood depths are normalized to 0-1 scale with 1 having the highest flood exposure and 0 have no flood exposure.

$$Exposure = \begin{cases} 0 & d_{max} = 0 & \textit{(No Flooding)} \\ 1 & 0.1 \le d_{max} \le 0.15 & \textit{(Ankle Deep)} \\ 2 & 0.15 < d_{max} \le 0.29 & \textit{(Lower than Knee)} \\ 3 & 0.29 < d_{max} \le 0.49 & \textit{(Knee)} \\ 4 & 0.49 < d_{max} \le 0.91 & \textit{(Waist)} \\ 5 & 0.91 < d_{max} \le 1.07 & \textit{(Chest)} \\ 6 & d_{max} > 1.07 & \textit{(Higher than Chest)} \end{cases} \tag{3}$$

4.2 Sociodemographic Vulnerability at the Parcel Level

Sociodemographic vulnerability data at the block group level was collected from Bixler et al. (2021), who utilized data from the 2017 ACS 5-Year Estimates. Bixler et al. (2021)'s procedure is an adaptation of SoVI® specifically developed for Austin, TX and Texas at large (Figure 3). Of the 29 SoVI variables, 4 were not available for this time period in Austin at the block group level and were therefore not extracted (hospitals per capita, percent of population without health insurance, nursing home residents per capita, percent female headed households). To further handle missing values, Bixler et al. (2021) excluded special use block groups (e.g., airports, military bases, prisons) and filled in holes by spatially interpolating from the surrounding block groups (Bixler et al., 2021). Min-max scaling all values for each block group further prepared the variables for the principal component analysis.

Figure 3. Procedure for calculating the Social Vulnerability Index (SVI).

The principal component analysis's (PCA) purpose is to reduce the dimensionality to statistically optimized components. A large number of variables are likely to have an influence on an individual's vulnerability. The PCA reduces variables to the most influential factors and merges them into similar highly correlated components. As a result, seven variables were eliminated, leaving a total of 18 variables divided into six components (Wealth, Language and Education, Elderly, Housing Status, Social Status and Gender). These 18 variables (Table 3) accounted for 74.48% of the observed variance. The cardinality of each component was adjusted so that a higher variable value indicated a higher vulnerability. For example, Wealth has a negative cardinality because having a higher per capita income would make an individual less vulnerable. The numerical composite social vulnerability score for each block group is the sum of the normalized and direction-adjusted values for each variable. This final score was again normalized from 0 to 1 (with one being the most vulnerable). The residential parcel SVI score is the SVI score for the block group to which that parcel belongs to.

$$Vulnerability = BG_{SVI} \in [0,1] \tag{4}$$

4.3 Flood Risk at the Parcel Level

As previously described, risk is the product of frequency, exposure, and vulnerability. Since this analysis focuses on a historical single event, frequency is set to 1, and

therefore household risk is calculated by multiplying the normalized flood exposure value (Eq. [3]) by the normalized relative sociodemographic vulnerability value (Eq. [4]). Plotted by quintile, the final residential parcel flood risk highlights the comparative communities that are the least and most at-risk.

$$Risk = Exposure * Vulnerability \qquad (5)$$

4.4 Pluvial Flooding Validation

GeoFlood has been shown to capture the general fluvial inundation patterns of flood events, with inundation extents overlapping with 60–90% of FEMA inundation extents (Zheng et al., 2018). To validate Fill-Spill-Merge and our pluvial inundation estimates, we employed a physically-based 2D hydrodynamic model by using the software ProMaIDes (Protection Measure against Inundation Decision Support). ProMaIDes is a modular open-source tool for the risk-based assessment for river, urban and coastal flooding and has been developed at the RWTH Aachen University and University Magdeburg-Stendal, Germany (Grimm et al., 2012; Bachmann, 2012, 2021). The hydrodynamic analysis implemented in ProMaIDes is based on a finite volume approach solving the diffusive wave equations and includes a multistep backward differentiation method for the temporal discretization (Tsai, 2003).

The 2D model domain for the hydrodynamic model is one subbasin within the Shoal Creek Watershed, covering approximately 5 km². Furthermore, an adaptive control method was used on the time increment. The hydrodynamic model can be driven by spatially and temporally varying rainfall input, however, to enhance comparability, a uniform rainfall depth of 13.2 cm was applied. Additionally, a uniform roughness coefficient for the model area of 0.03 (Manning) was used. To avoid high computational costs, the simulation time was limited to 1-hour of rainfall and 5-hours of follow up time, and the DEMs resolution was down sampled to 3-meter by 3-meter cells. The computational time required was 670 minutes using an AMD Ryzen 9 3900X 12-Core Processor. The model's final inundation output was then put through the same reclassification scheme to determine parcel level exposure (Eq. [3]). We compared the parcel level exposure values of our terrain-based estimate to the model's final inundation output for all parcels in this subbasin that are not impacted by fluvial flood waters (3,015 parcels).

Table 3. Variables included and excluded from the Social Vulnerability Index (SVI) of Austin, Texas, retrieved from Bixler et al. (2021).

Variable	Component	Cardinality	Variance Explained (%)
Percent households earning over $200,000 annually Median housing value Per capita income Median gross rent	Wealth	(-)	17.53%
English as a second language with limited proficiency Percent with less than 12th grade education Percent Hispanic	Language and Education	(+)	14.51%
Percent households receiving social security benefits Percent population under 5 years or 65 and over Median age	Elderly	(+)	12.17%
Percent children living in 2-parent families Percent civilian unemployment	Housing Status	(+)	11.91%
Percent of housing units with no car Percent civilian unemployment Percent Poverty Percent Black	Social Status	(+)	9.61%
Percent female participation in labor force Percent female	Gender	(+)	8.75%
Percent of population without health insurance Nursing home residents per capita Percent female headed households Hospitals per capita	Removed due to lack of BG data	NA	NA
Percent employment in extractive industries Percent employment in service industry Percent unoccupied housing units Percent Native American Percent mobile homes Percent renters Percent Asian	Removed during PCA	NA	NA
	TOTAL Variance Explained		**74.48%**

5 Results

In the following figures (excluding Figure 4), inset areas (A) and (B) compare two different locations within Austin, TX and represent the same area across all figures. Inset (A) to the North highlights an area that is dominated by fluvial flooding. Inset (B) to the South highlights an area that is dominated by pluvial flooding.

5.1 Pluvial Flooding Validation

To compare the inundation extent estimates from Fill-Spill-Merge to the physical based model, both rasters were overlayed and intersected (Figure 4). The intersected raster was then classified into four categories of wet-wet, wet-dry, dry-wet, and dry-dry, with each term in each pair referring to one of the raster layers (i.e., wet-wet refers to a cell that is flooded in both rasters, where wet-dry refers to a cell that is flooded in only one raster) (Johnson et al., 2019). Accuracy is then defined as the number of wet-wet cells divided by the sum of the wet-wet, wet-dry, and dry-wet cells. The Fill-Spill-Merge and physical based model were found to be 31% accurate when excluding any inundated depths less than 1-cm. When the lower limit of allowable depths is increased to 6-cm and 15-cm, the accuracy increases to 44% and 66.5% respectively, suggesting that Fill-Spill-Merge performs comparably well at greater depths. Fill-Spill-Merge is predominantly under-estimating inundated extents when compared to the model, and this is occurring at larger intersections and along some roadways (Figure 4, inset A, B, C).

Comparing our reclassified parcel level pluvial flood exposure estimates to that of a hydrodynamic model's output, we classified 92% of the 3,015 parcels similarly (Figure 4). Of the 251 misclassified parcels, 94.4% (237 parcels) of them were misclassified by only one class (Eq. [3]). For example, a residential parcel may have an exposure classification of 2 (between 0.15 and 0.29 m of flooding) in the model output, but only an exposure classification of 1 (between 0.01 and 0.15 m of flooding) in the Fill-Spill-Merge estimate. Furthermore, of the misclassified parcels, 69% (173 parcels) of them involve a misclassification between no flooding, and less than 15-cm of flooding, the lowest exposure level. Therefore, the misclassified parcels have a minimal impact on final risk values across the subbasin. Misclassifications are not specifically concentrated in any one area and appear across the subbasin.

5.2 Flood Exposure

Through the application of our workflow (Figure 2) we estimated the worst-case fluvial and pluvial flood extent for the Memorial Day Flood (Figure 5). Pluvial and fluvial flooding do not affect all locations equally, with some locations being affected more by fluvial flooding that follows streamlines (inset A1) and others being affected more by pluvial flooding along roadways and in between parcels (inset B1). Furthermore, the compounding mechanism varies across the study region, with some locations experiencing both fluvial and pluvial flooding in time and space (Inset A2) and other locations compounding only in time (Inset B2).

Floodwater extents increase when considering both pluvial and fluvial sources (Figure 6). Of the 177 block groups within the study area, 67 (37.9%) experience flooding from only pluvial sources, while flood mapping that exclusively considers fluvial sources would not identify these block groups' flood exposure. Only five block groups have an increase in flood extents greater than 100%, suggesting that while pluvial flooding can greatly increase inundation extents, fluvial flooding remains the dominant source of flood waters (i.e., the majority of flooding comes from fluvial sources) in those block groups that experience fluvial flooding. This increase in floodwater extents is also visible by catchment area, showing that the increase in floodwater extents is equally substantial across an entire watershed and not limited to certain locations along a stream reach (Table 4).

509 The increase in floodwater extents within catchment areas when considering the com-
510 bined effects of fluvial and pluvial flood sources ranges from 40% to 156%.

Table 4. Percent increase in inundation extent by catchment area when comparing fluvial/pluvial flooding with only fluvial sources during the 2015 Memorial day Flood in Austin, Texas.

Catchment Name	Area (km^2)	Fluvial Inun. Area (km^2)	Pluvial Inun. Area (km^2)	Percent Fluvial Inun.	Percent Compound Inun.	Percent Increase Inun. Area
Walnut Creek (L)	52.7	5.37	4.73	10.2%	17.5%	71.3%
Walnut Creek (M)	35.0	4.04	2.57	11.5%	17.1%	47.9%
Walnut Creek (U)	41.7	6.22	4.18	14.9%	22.5%	50.6%
Boggy Creek	34.4	1.93	3.36	5.6%	14.4%	156.0%
Shoal Creek	33.9	4.59	2.58	13.5%	19.3%	42.3%
Waller Creek	14.3	1.48	1.12	10.4%	16.7%	61.4%
Colorado River (L)	24.0	2.97	4.50	12.4%	30.3%	145.3%
Colorado River (U)	19.6	2.07	0.91	10.5%	14.9%	41.1%

511 Analyzing flood exposure results by block groups produces a high level of variabil-
512 ity, both between and within block groups (Figure 7). High coefficients of variation (stan-
513 dard deviation divided by mean) signals a wide distribution, suggesting that mean ex-
514 posure within the giving boundary is going to significantly over- and under- estimate house-
515 hold exposure. Furthermore, the high dispersion in average depths by block group sug-
516 gests that aggregating at a higher-level boundary (e.g., county) would result in similarly
517 high coefficients of variation.

518 Reporting exposure values by residential parcels allows for this variability and dis-
519 persion to be captured in the final risk calculation (Figure 8). The reclassification of ex-
520 posure values (Eq. [3]) allows for easier comparisons between regions, thus allowing for
521 quicker identification of potential hot spots. High exposure results appear predominantly
522 along streamlines, which is expected as fluvial channel floodplains offer more locations
523 for higher depths as compared to topographic depressions which have a much smaller
524 scale in size. The final risk calculation uses these exposure estimates.

5.3 Sociodemographic Vulnerability

526 Clear geographic disparities exist between the eastern and western portions of the
527 study area in terms of the SVI estimates (Figure 9). Each residential parcel's SVI value
528 is equivalent to the SVI value of the block group that it coincides with. It is important
529 to remember that the SVI estimate shown is relative and is therefore an arbitrary value
530 that can be compared between locations. Parcels with a score of 1 are the most vulner-
531 able, and parcels with a score of 0 are the least vulnerable.

5.4 Risk

533 There is a clear distinction of risk between the east and west portions of the study
534 area, however individual block groups themselves also contain variability (Figure 10).
535 Some locations have varying levels of risk within the same block group, which aggregated
536 risk estimates would not capture. This is especially prevalent in areas with a higher con-
537 centration of higher risk households. Furthermore, high risk parcels exist in areas not
538 directly adjacent to stream reaches.

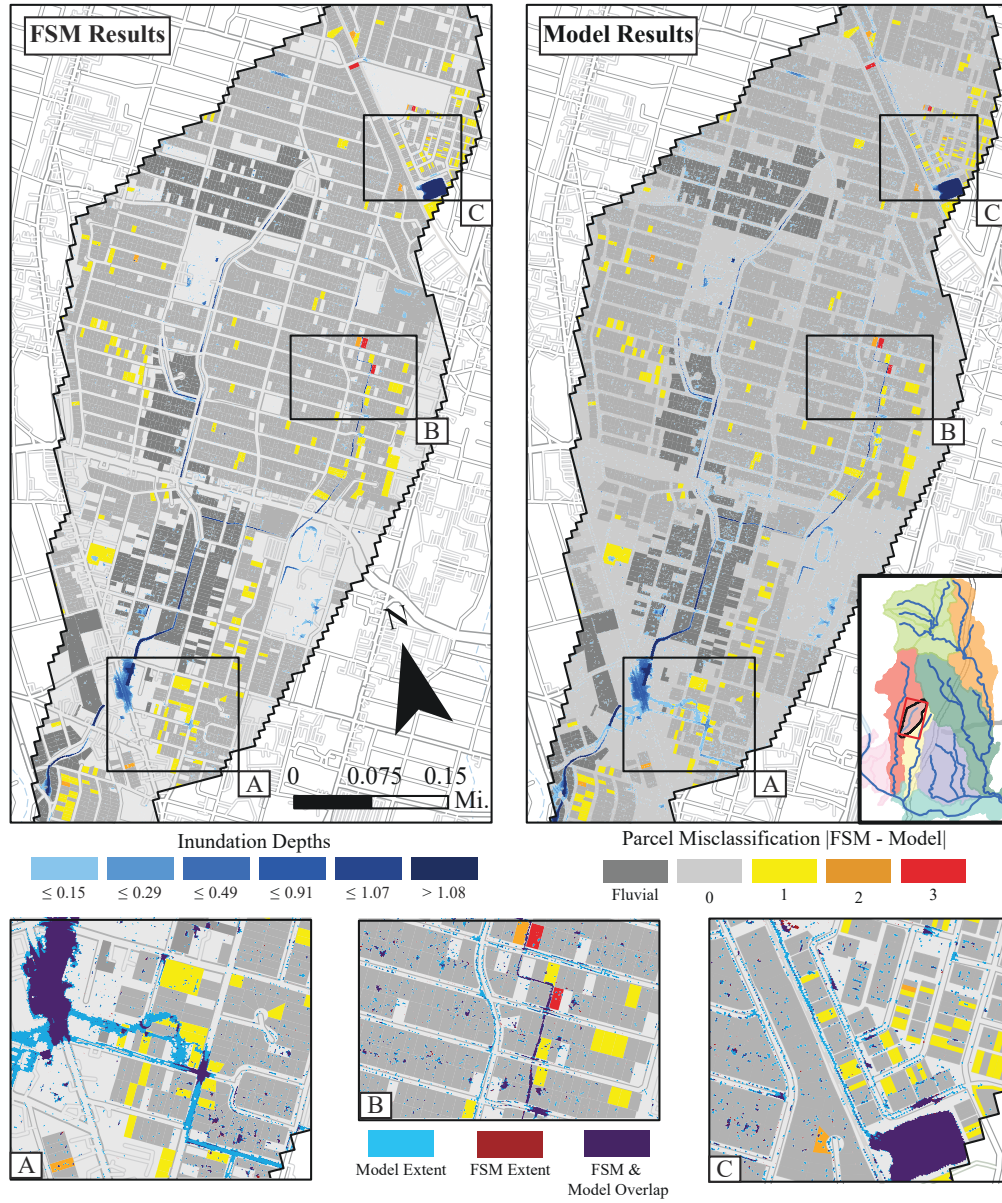## FSM's and Hydrodynamic Model's Parcel Classification Comparison

Figure 4. Comparison between near-real time estimate (Fill-Spill-Merge) and a 2D physical based hydrodynamic model estimate of pluvial flooding at the parcel level. (A), (B), and (C) highlight areas with concentrated parcel misclassifications.
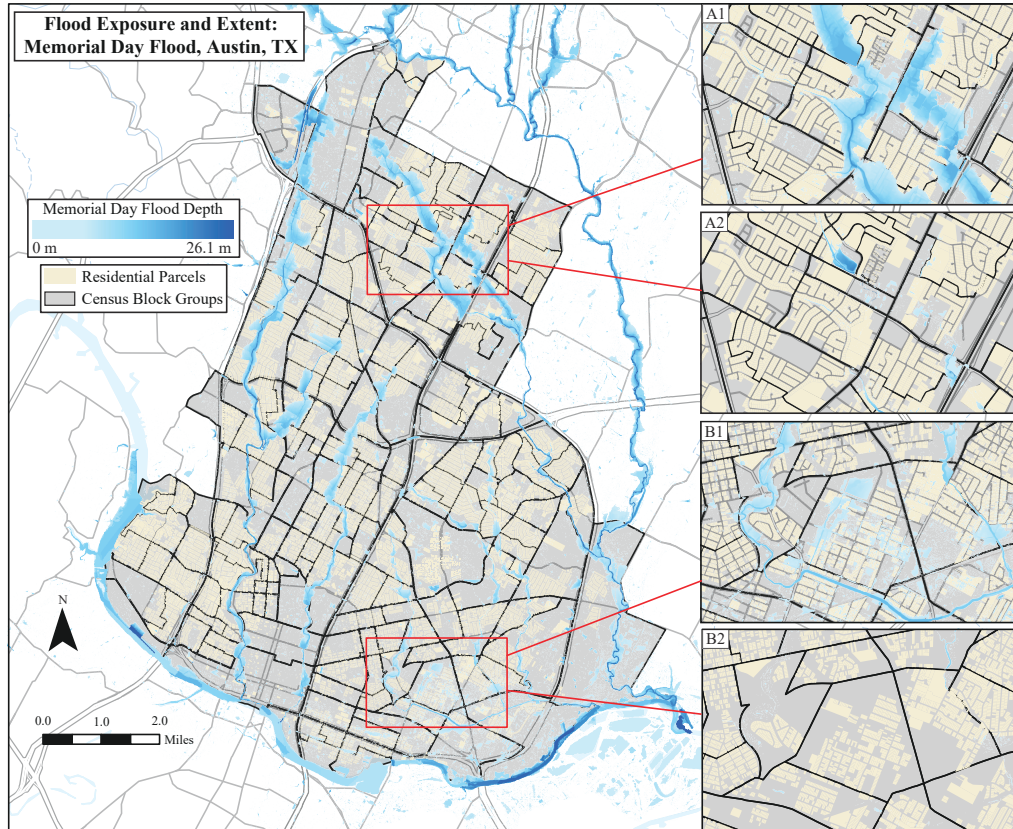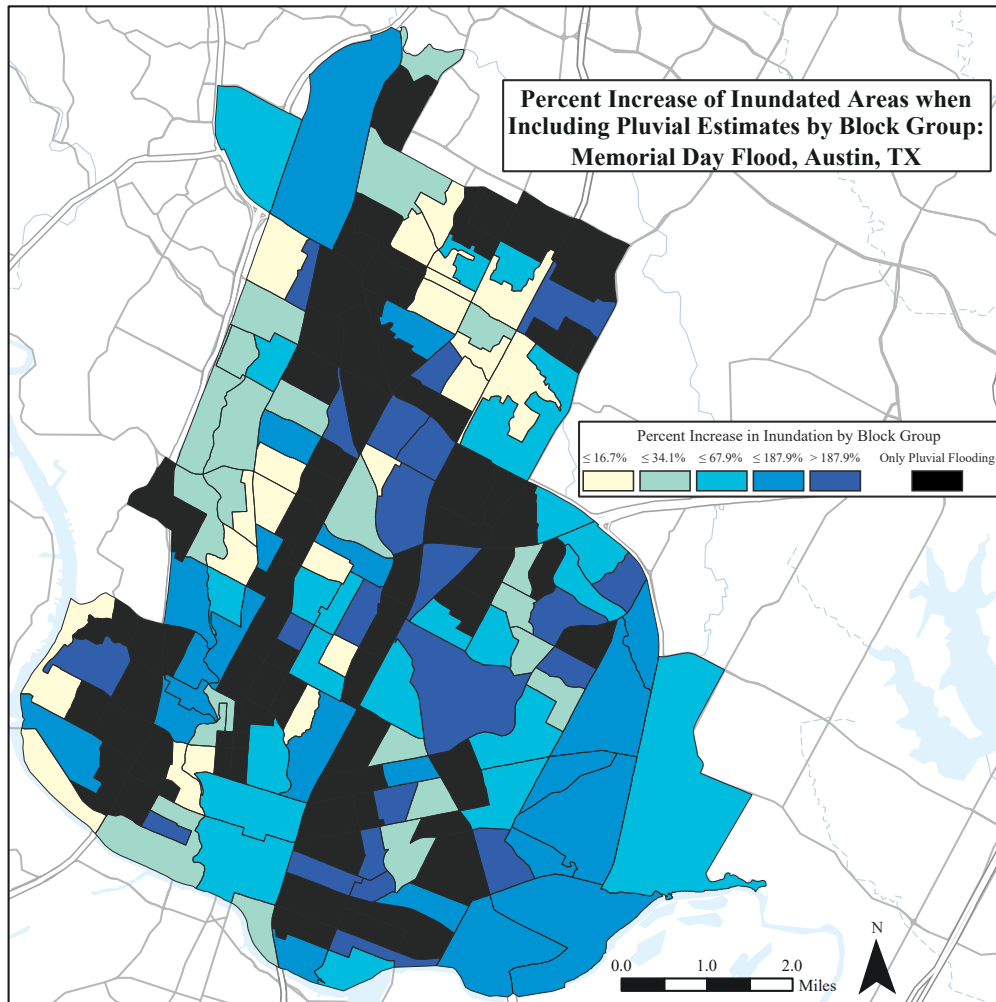
Figure 5. Fluvial and Pluvial flood depths and extent in Austin, Texas during the 2015 Memorial Day Flood. Insets A1 and B1 show the worst-case inundation estimates for two different locations. Insets A2 and B2 show those same locations, but only show inundation extents that are from the overlapping impacts of fluvial and pluvial flooding (i.e., the extent shown in A2 and B2 highlights the specific locations that experience both fluvial and pluvial flooding.

Figure 6. Percent increase in inundation extent by Census Block Group when comparing fluvial/pluvial flooding with only fluvial sources during the 2015 Memorial day Flood in Austin, Texas.

Figure 7. Average flood exposure depth of residential parcels and their coefficient of variation by Census Block Group during the 2015 Memorial day Flood in Austin, Texas.
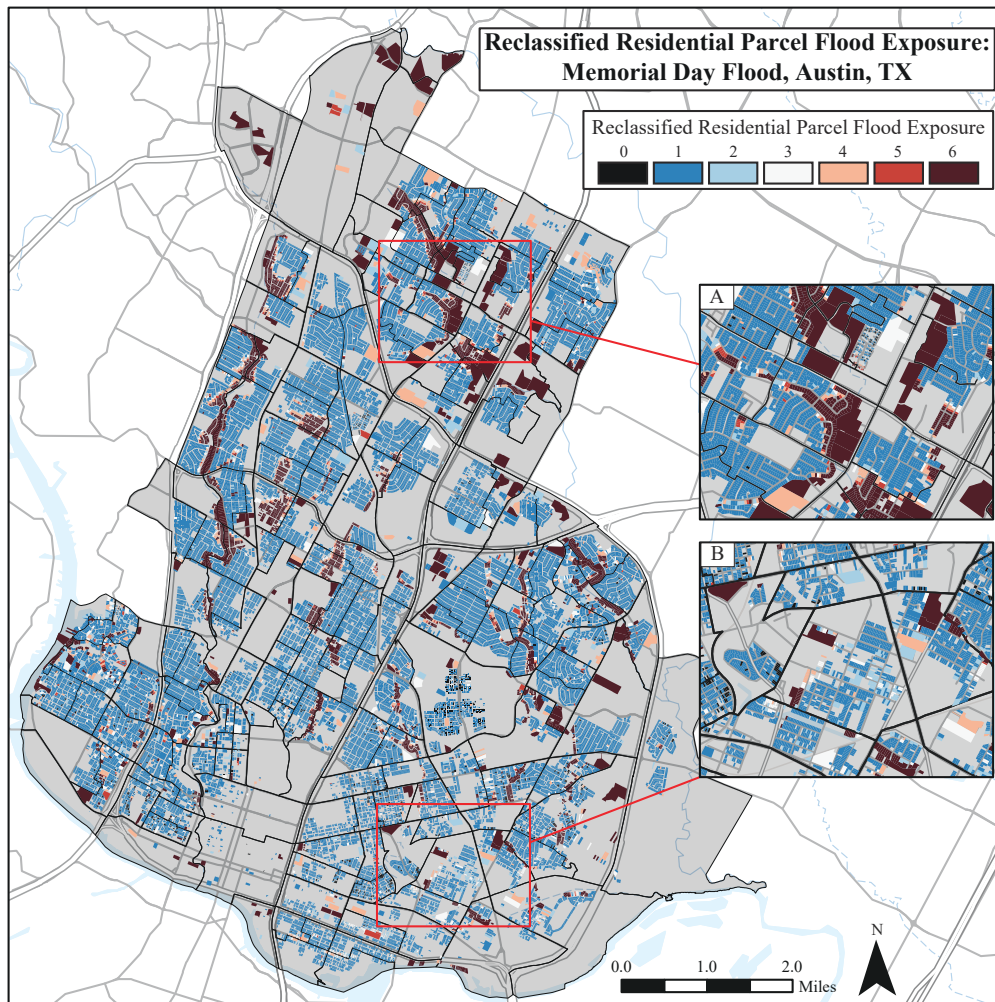
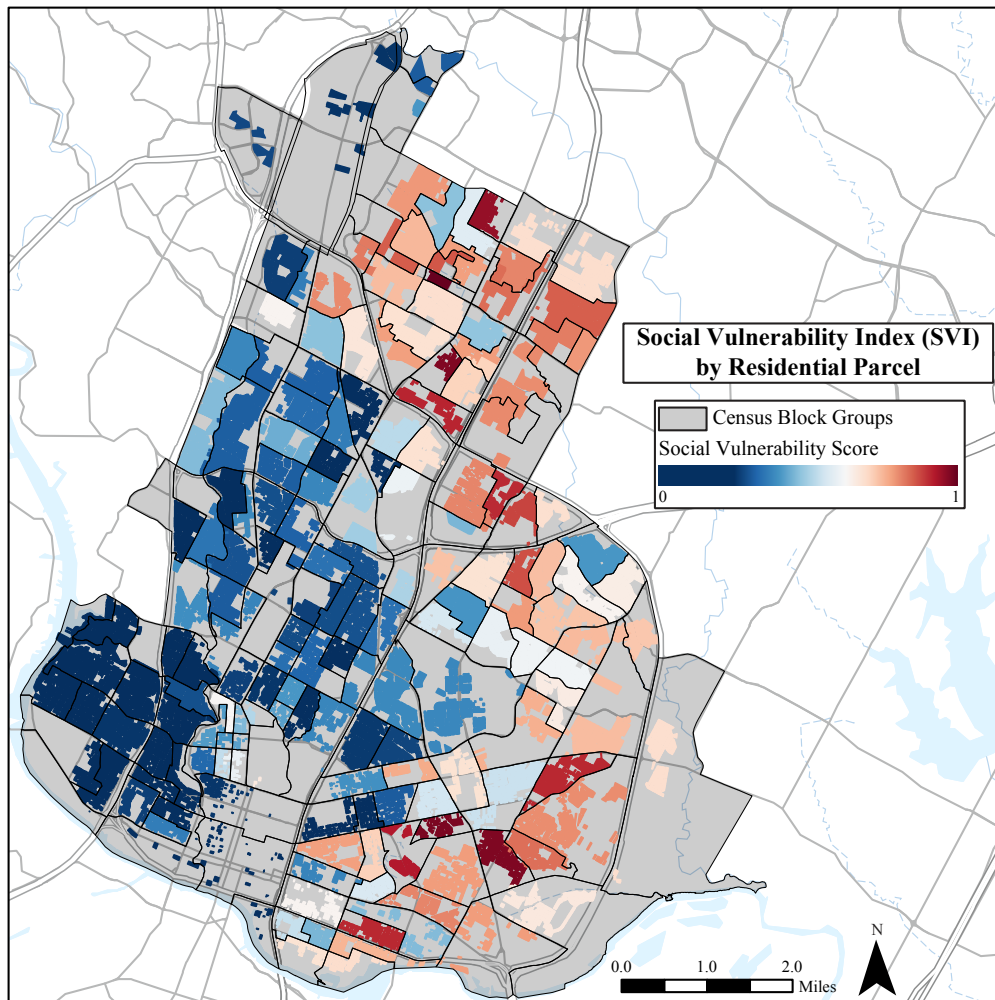**Figure 8.** Reclassified residential flood exposure during the 2015 Memorial day Flood in Austin, Texas.

Figure 9. Austin, Texas relative Social Vulnerability Index (SVI), with 1 being most vulnerable and 0 being least vulnerable.
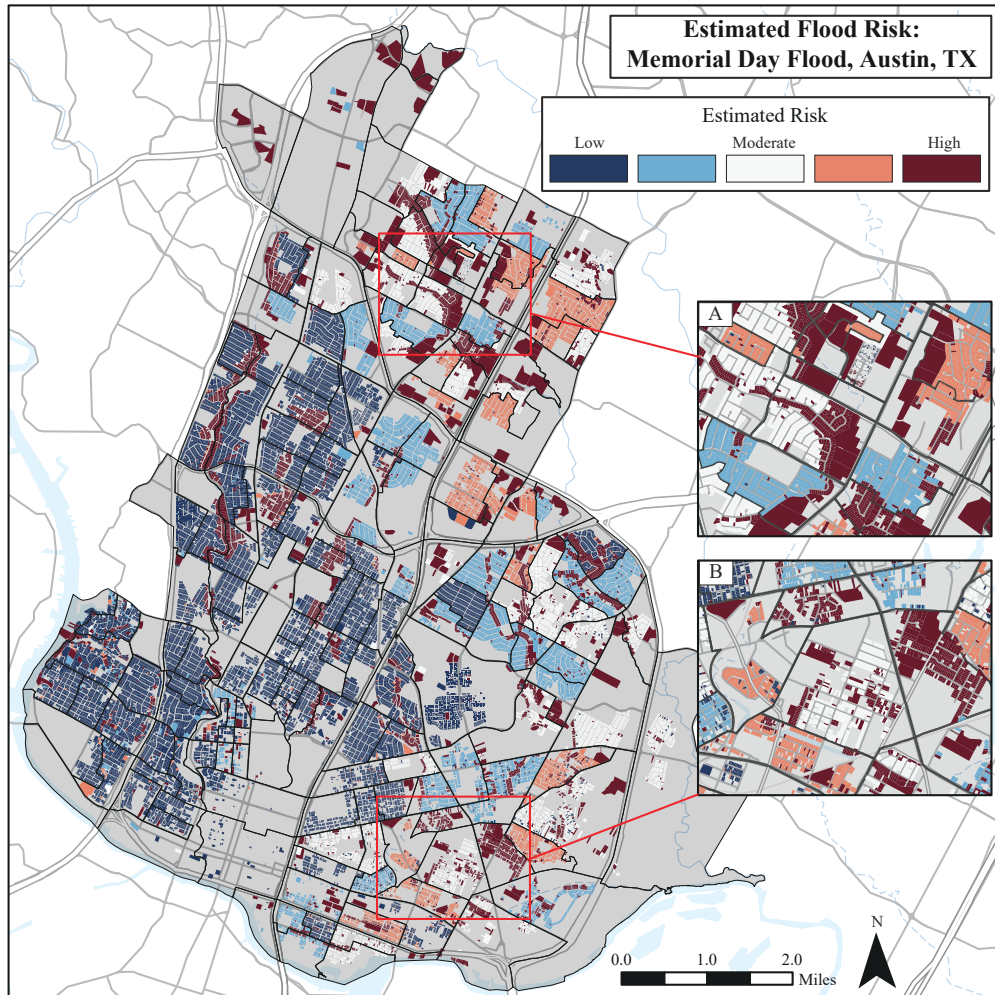
Figure 10. Residential flood risk during the 2015 Memorial Day Flood in Austin, Texas.

6 Discussion

6.1 High-Resolution Compound Flooding's Role in Increasing Parcel Level Exposure

Flood exposure is a function of both inundation extents and depths. Extent determines the breadth of flood waters, with larger flood extents forcing response and recovery efforts to spread out over large areas. Depth determines the level of damage, with a higher depth correlated with a higher level of damage. A significant source of exposure in urban areas that is often ignored is from pluvial sources (Houston et al., 2011; Grahn & Nyberg, 2017). The exclusion of pluvial flooding from flood mitigation planning will result in a drastic under representation of flood water extents which could impact millions of households across the United States (Wing et al., 2018). With 38% of all Census Block Groups in our study area only impacted by pluvial flooding, our results show that pluvial flooding cannot be excluded from flood hazard maps (Figure 6).

Leading flood hazard maps (e.g., FEMA floodplain maps) and numerous flood risk studies (C. Burton & Cutter, 2008; Fekete, 2009; C. G. Burton, 2010; Finch et al., 2010; Abbas & Routray, 2014; Chakraborty et al., 2014; Tate et al., 2016) do not consider pluvial flood waters in their inundation estimations, focusing on fluvial and/or coastal flooding. Recent national level exploratory analyses that do consider pluvial flood waters rely on coarse resolution (30-meter) estimates (Wing et al., 2018; Tate et al., 2021), which can fail to capture small scale topographic depressions that exist in urban environments. For example, the average width of a 4-lane intersection is approximately 15-meters. At 30-meter resolution, it will not be possible to capture pluvial flooding's impact on roadways. We show that pluvial flooding specifically leads to ponded water on impervious surfaces such as roadways, intersections, and parking lots, that would otherwise not be identified as being inundated (Figure 5). Standing water depths greater than 13-cm can be high enough to reach the undercarriage of most passenger cars, inhibiting safe evacuation routes (Moftakhari et al., 2018). Any increase in velocity or depth can block emergency response vehicles from reaching inundated areas.

The co-occurrence of multiple types of flooding while usually considered with respect to coastal flooding (Wahl et al., 2015), can be translated to inland urban areas as either predominantly increasing depths (i.e., occurring at the same location) or extents (i.e., occurring at the same time). In our study area, compound flooding is predominantly related to increasing extents (Figure 5). Fluvial flooding is associated with higher depths, concentrated along stream reaches, while pluvial flooding is associated with lower depths spread out over larger areas (Figure 8). Low depth pluvial flooding can be described as "nuisance flooding", which has the ability to disrupt transportation networks, impact public safety, and potentially damage property (Moftakhari et al., 2018). Fluvial and pluvial floodwaters require specific mitigation actions; therefore, it is important to quantify this distinction due to the place-based nature of flooding.

The City of Austin's FloodPro software, which is the city's leading source of floodplain information, lacks pluvial flooding information, therefore significantly under reporting exposure. The inclusion of high-resolution pluvial flooding estimates is necessary in understanding the potential impacts to local emergency services and infrastructure. High-resolution compound flooding estimates can drastically improve local and regional flood polices' impacts by more accurately addressing flood issues that would otherwise go unnoticed.

6.2 Impact of Aggregating Exposure and Risk to Cartographic Boundaries

One of the leading purposes of mapping flood exposure with social vulnerability is to identify the most at-risk populations. However, aggregating and reporting estimates

to cartographic boundaries can significantly mask household level variability, thus misclassifying some high- and low-risk households. This misidentification can inhibit the proper allocation of mitigation and emergency response services. Our results show that when household exposure depths are averaged to Census Block Groups, 80% of all Block Groups have a coefficient of variation higher than 100%, showing that using a central tendency statistic to report flood exposure over a cartographic boundary is not representative of actual flood conditions (Figure 8).

The majority of recent research on social vulnerability to floods aggregates exposure and subsequent risk estimates to Census Tract, zip code, or county boundaries (C. Burton & Cutter, 2008; Cutter et al., 2013; Chakraborty et al., 2014; Wing et al., 2020; Tate et al., 2021).The two primary reasons for aggregating exposure are (i) the exploratory nature of these studies to identify broad regions of risk and (ii) the aggregated boundary is the resolution of the utilized socio-economic data. Exposure and risk are heterogeneous within block groups (Figure 8 and 10). Since social vulnerability estimates do not vary within a block group (Figure 9), the observed heterogeneity in the final risk estimate comes solely from the variability in exposure. While aggregated results can draw attention to broad regions of risk, household level data is required to properly classify who is at risk. This is not the first study to incorporate tax parcel data to attempt to estimate risk at the household level (Nelson et al., 2015; Fahy et al., 2019), however previous studies have relied on 100-year floodplain data that lack pluvial estimates. With pluvial flooding having specific small-scale impacts, such as ponding along roads and intersections, using higher resolution socioeconomic data requires an equivalent increase in resolution of inundation estimates.

Mitigation policies and programs exist at nearly all levels of government, including national, state, and local programs (e.g., FEMA's National Flood Insurance Program, Texas Water Development Board's Flood Intended Use Program, and the City of Austin's Climate Resilience Action Plan). While broad exploratory and aggregated studies can assist with equally scaled programs at the national and state level, high resolution household estimates are necessary for local mitigation plans to effectively serve those most at risk. Optimizing the location of local flood mitigation efforts based on a complete flood exposure analysis (high resolution pluvial and fluvial flooding) at the household level can further maximize a city's social return on investment. If our final risk estimates were aggregated to the block group level, high risk households would be masked and not identified. Similarly, low risk households could be labeled inaccurately as high risk, thus leading to a misappropriation of resources. High risk households are not necessarily limited to high vulnerability neighborhoods, and it is therefore important to view and report risk estimates in an unbiased manner.

6.3 Pluvial Flooding Validation

The methodology employed by this study uses terrain-based flood mapping (GeoFlood and Fill-Spill-Merge) to produce inundation estimates in near-real time and is not intended to replace more complex physical based hydrodynamic models, rather it can produce a storm-specific estimate of risk as a storm event occurs. While GeoFlood's accuracy has already been researched (Zheng et al., 2018), Fill-Spill-Merge's applicability as a pluvial flooding estimate has previously not been studied. The advantages and disadvantages between a terrain-based estimate of pluvial flooding to a hydrodynamic model can be grouped into two categories: time and accuracy.

The single subbasin used in the hydrodynamic model, which is 5 km^2 in size, represents only 2% of the entire watershed studied and took over 11 hours to compute. This is even considering the additional model parameters chosen to reduce computational time such as using a uniform rainfall and roughness coefficient, reduced rainfall and follow up time, and down sampling the DEM. While there is room for the model to be optimized

and be increased in speed, the terrain-based estimate for the entire study area can be processed in a few minutes. Flash floods, especially those occurring in urban areas can occur within six hours of initial rainfall, and are some of the most hazardous natural events (Hapuarachchi et al., 2011). Short-term storm specific risk estimates require the speed that comes with our estimation methodology, which can play a critical role in deploying emergency communications before a flooding event begins.

When we compared the terrain based pluvial inundation estimate to the hydrodynamic model, we found that it had a spatial extent accuracy of 31%, which further increased to 66.5% when we ignored the lowest depth classification which would likely not be deep enough to inhibit vehicular traffic and therefore have minimal effects (Eq. [3]). The mismatch in inundation extents predominantly occurred along intersections and roadways, which does not have an impact on our household level classification since these locations do not intersect with residential parcels. This suggests that Fill-Spill-Merge can potentially play a role in estimating infrastructure service interruptions (e.g., road closures, emergency vehicles being blocked) in future network studies, while still serving its purpose of estimating household risk for this study. This is supported by our 92% similar household classification, especially considering 237 of the 251 misclassified parcels were by only one class. The difference in the depth estimates of Fill-Spill-Merge and the hydrodynamic model are minimized when we examine maximum parcel depths and aggregate our results to these boundaries. Identifying the highest risk households is the most important function of the reclassification methodology and showing that 69% of the misclassified houses are between no flooding and less than 15-cm of flooding will have little to no effect on the final risk estimates.

6.4 Equity and Environmental Justice Implications

There is a growing concern regarding the inequitable distribution of flood risk across vulnerable populations as flooding is broadly projected to increase in frequency and intensity (Tate et al., 2021). Furthermore, there is limited research at the intersection of flood risk and environmental justice at the household level (Collins et al., 2015). Our results presented highlight important areas for further research to better conceptualize and measure flood inequity, including the distribution of pluvial flooding across diverse urban communities and downscaling risk estimates below census block groups.

Flood inequity may be present in numerous states, regions, and cities but it is far from uniform across all areas (Collins et al., 2018). While some studies show that flood exposure is higher for socially vulnerable populations (Lee & Jung, 2014; Rolfe et al., 2020), other studies show that low socially vulnerable populations can experience the highest exposure to flood hazards given certain circumstances (Fielding & Burningham, 2005; Bin & Kruse, 2006; Ueland & Warf, 2006; Chakraborty et al., 2014). It is because of these differences from one city or one flood event to another that having an event specific understanding of vulnerability and exposure at the highest resolution possible can provide valuable information to enact proper preparedness and response measures. Missed exposure from the lack of high-resolution pluvial inundation estimates or the masking of household level variability in exposure can unintentionally perpetuate systemic risk in a city and thus becomes an important environmental justice concern.

6.5 Limitations and Future Work

There are inherent challenges associated with SVIs and reporting results in terms of relative risk that will require future and more in-depth analyses. The simplistic nature of SVIs allows instantaneous estimations, but they cannot measure the full complex nature of vulnerability (Rufat et al., 2015). SVIs could inadvertently weight variables inaccurately, creating a biased depiction of vulnerability over a region, thus misidentifying at risk individuals and perpetuating risk. SVIs should incorporate local knowl-

edge, including variables such as distance to critical infrastructure (e.g., hospitals) or access to resources (e.g., gas, food, electricity, transportation, and water), to ensure proper representation of all residents. Further consideration needs to be given to estimating social vulnerability at the household level. Census data, especially at the Block Group level, can have large margins of error. Assuming values found for the areal units apply at the household level requires a more specific analysis. One such option that has been used to address this concern is the use of primary household survey data (Collins et al., 2015).

There are also challenges associated with estimating flood exposure. The methods used to estimate exposure are a simplification of much more complex flood mechanics and do not account for such variables as storm drainage networks, movement around buildings and structures, and timing/velocity considerations. While this workflow can produce estimates in near-real time, it is important to consider these estimates in the broader context of flood modeling and consider the inherent uncertainties of terrain-based flood mapping. In the context of pluvial flooding, specifically nuisance flooding at lower depths, estimates are directly impacted by DEM accuracy. The DEM used has a vertical accuracy of 6-cm, which is significant when considering flood depths that are between 3 and 10-cm (Moftakhari et al., 2018). While uncertainty and its communication can have a substantial impacts on regulatory and response processes (Downton et al., 2005; Luke et al., 2018), there is also evidence that flood emergency managers are willing to trade larger uncertainties for faster information (McCarthy et al., 2007).

While it is necessary to understand both short-term and long-term risk, as they require unique actions and policies to address them, this study is a specific attempt to identify short-term risk for a known storm event. Long term future flood risks caused by the projected increase in frequency of extreme weather events due to climate change will require their own analyses. Future flood risk calculations can incorporate this workflow by using modeled storm characteristics and projected sociodemographic information. As a supplemental tool, this workflow can contribute to other research, response, and mitigation efforts.

7 Conclusion

The proposed workflow in this paper identifies storm specific urban flood risk at the parcel level using high resolution topographic data, pluvial and fluvial flood estimations, and a localized social vulnerability index. The application of this workflow to the Memorial Day Flood in Austin, TX showed that estimating fluvial flooding alone is not enough to predict urban flood exposure and that incorporating high resolution sociodemographic information is important in identifying local variability in vulnerability. Furthermore, aggregating results to cartographic boundaries masks the dispersion of exposure, vulnerability, and risk thus making it difficult to identify priority locations for remediation, mitigation, and response. Additionally, our pluvial inundation estimates classified household pluvial flood exposure accurately 94.4% of the time. Including more flooding and vulnerability factors, such as non-census sociodemographic data, social and government networks, and local infrastructure data will improve risk estimations.

If this manuscript is accepted, all data used and the associated codes will be made available in a public repository by the time of publication.

References

Abbas, H. B., & Routray, J. K. (2014). Vulnerability to flood-induced public health risks in Sudan. *Disaster Prevention and Management*, *23*(4), 395–419. doi: 10.1108/DPM-07-2013-0112

Ahmed, F., Khan, M. S. A., Warner, J., Moors, E., & Terwisscha Van Scheltinga, C. (2018). Integrated Adaptation Tipping Points(IATPs) for urban flood resilience. *Environment and Urbanization*, *30*(2), 575–596. doi: 10.1177/0956247818776510

Ahmed, F., Moors, E., Khan, M. S. A., Warner, J., & Terwisscha van Scheltinga, C. (2018). Tipping points in adaptation to urban flooding under climate change and urban growth: The case of the Dhaka megacity. *Land Use Policy*, *79*(April), 496–506. doi: 10.1016/j.landusepol.2018.05.051

Alfieri, L., Bisselink, B., Dottori, F., Naumann, G., de Roo, A., Salamon, P., . . . Feyen, L. (2017). Global projections of river flood risk in a warmer world. *Earth's Future*, *5*(2), 171–182. doi: 10.1002/2016EF000485

Arnell, N. W., & Gosling, S. N. (2016). The impacts of climate change on river flood risk at the global scale. *Climatic Change*, *134*(3), 387–401. doi: 10.1007/s10584-014-1084-5

Bachmann, D. (2012). *Beitrag zur entwicklung eines entscheidungsunterstützungssystems zur bewertung und planung von hochwasserschutzmaßnahmen* (Unpublished doctoral dissertation). Institut für Wasserbau und Wasserwirtschaft, RWTH Aachen.

Bachmann, D. (2021). *ProMaIDes: State-of-the Science Flood Risk Management Tool.* Institute of Hydraulic Engineering and Water Resources Management. Retrieved from https://promaides.h2.de/promaides/

Barnes, R., Callaghan, K., & Wickert, A. (2019b). Computing water flow through complex landscapes - Part 3: Fill-Spill-Merge: Flow routing in depression hierarchies. *Earth Surface Dynamics*, *7*(3), 737–753. doi: 10.5194/esurf-7-737-2019

Barnes, R., Callaghan, K. L., & Wickert, A. D. (2019a). Computing water flow through complex landscapes, Part 2: Finding hierarchies in depressions and morphological segmentations. *Earth Surface Dynamics*, *7*(3), 737–753. doi: 10.5194/esurf-7-737-2019

Bin, O., & Kruse, J. B. (2006). Real Estate Market Response to Coastal Flood Hazards. *Natural Hazards Review*, *7*(4), 137–144. doi: 10.1061/(asce)1527-6988(2006)7:4(137)

Bixler, P., Yang, E., Richter, S., & Coudert, M. (2021). *Co-production for urban resilience: A multi-hazard approach in Austin, Texas.*

Burton, C., & Cutter, S. L. (2008). Levee Failures and Social Vulnerability in the Sacramento-San Joaquin Delta Area, California. *Natural Hazards Review*, *9*(3), 136–149. doi: 10.1061/(asce)1527-6988(2008)9:3(136)

Burton, C. G. (2010). Social Vulnerability and Hurricane Impact Modeling. *Natural Hazards Review*, *11*(2), 58–68. doi: 10.1061/(asce)1527-6988(2010)11:2(58)

Calianno, M., Ruin, I., & Gourley, J. J. (2013). Supplementing flash flood reports with impact classifications. *Journal of Hydrology*, *477*, 1–16. doi: 10.1016/j.jhydrol.2012.09.036

Callaghan, K. L., & Wickert, A. D. (2019). Computing water flow through complex landscapes – Part 1: Incorporating depressions in flow routing using FlowFill. *Earth Surface Dynamics*, *7*(3), 737–753. doi: 10.5194/esurf-7-737-2019

Cardona, O. D., Van Aalst, M. K., Birkmann, J., Fordham, M., Mc Gregor, G., Rosa, P., . . . Thomalla, F. (2012). Determinants of risk: Exposure and vul-

nerability. In *Managing the risks of extreme events and disasters to advance climate change adaptation: Special report of the intergovernmental panel on climate change* (pp. 65–108). Cambridge Univesity Press, Cambridge, UK, and New York, NY, USA. doi: 10.1017/CBO9781139177245.005

Chakraborty, J., Collins, T. W., Montgomery, M. C., & Grineski, S. E. (2014). Social and Spatial Inequities in Exposure to Flood Risk in Miami, Florida. *Natural Hazards Review*, *15*(3), 04014006. doi: 10.1061/(asce)nh.1527-6996 .0000140

Chu, X., Yang, J., Chi, Y., & Zhang, J. (2013). Dynamic puddle delineation and modeling of puddle-to-puddle filling-spilling-merging-splitting overland flow processes. *Water Resources Research*, *49*(6), 3825–3829. doi: 10.1002/wrcr.20286

Collins, T. W., Grineski, S. E., & Chakraborty, J. (2018). Environmental injustice and flood risk: a conceptual model and case comparison of metropolitan Miami and Houston, USA. *Regional Environmental Change*, *18*(2), 311–323. doi: 10.1007/s10113-017-1121-9

Collins, T. W., Grineski, S. E., Chakraborty, J., & Flores, A. B. (2019). Environmental injustice and Hurricane Harvey: A household-level study of socially disparate flood exposures in Greater Houston, Texas, USA. *Environmental Research*, *179*(September), 108772. doi: 10.1016/j.envres.2019.108772

Collins, T. W., Grineski, S. E., Chakraborty, J., Montgomery, M. C., & Hernandez, M. (2015). Downscaling Environmental Justice Analysis: Determinants of Household-Level Hazardous Air Pollutant Exposure in Greater Houston. *Annals of the Association of American Geographers*, *105*(4), 684–703. doi: 10.1080/00045608.2015.1050754

Cutter, S. L., Boruff, B., & Shirley, W. L. (2003). Social vulnerability to environmental hazards. *Social Science Quarterly*, *84*(2), 242–261. doi: 10.1111/1540 -6237.8402002

Cutter, S. L., Emrich, C. T., Morath, D. P., & Dunning, C. M. (2013). Integrating social vulnerability into federal flood risk management planning. *Journal of Flood Risk Management*, *6*(4), 332–344. doi: 10.1111/jfr3.12018

de Carvalho Júnior, O. A., Guimarães, R. F., Montgomery, D. R., Gillespie, A. R., Gomes, R. A. T., Martins, É. d. S., & Silva, N. C. (2013). Karst depression detection using ASTER, ALOS/PRISM and SRTM-derived digital elevation models in the Bambuí group, Brazil. *Remote Sensing*, *6*(1), 330–351. doi: 10.3390/rs6010330

de Moel, H., & Aerts, J. C. (2011). Effect of uncertainty in land use, damage models and inundation depth on flood damage estimates. *Natural Hazards*, *58*(1), 407–425. doi: 10.1007/s11069-010-9675-6

Downton, M. W., Morss, R. E., Wilhelmi, O. V., Gruntfest, E., & Higgins, M. L. (2005). Interactions between scientific uncertainty and flood management decisions: Two case studies in Colorado. *Environmental Hazards*, *6*(3), 134–146. doi: 10.1016/j.hazards.2006.05.003

Fahy, B., Brenneman, E., Chang, H., & Shandas, V. (2019). Spatial analysis of urban flooding and extreme heat hazard potential in Portland, OR. *International Journal of Disaster Risk Reduction*, *39*(September 2018), 101117. doi: 10.1016/j.ijdrr.2019.101117

Falconer, R. H., Cobby, D., Smyth, P., Astle, G., Dent, J., & Golding, B. (2009). Pluvial flooding: New approaches in flood warning, mapping and risk management. *Journal of Flood Risk Management*, *2*(3), 198–208. doi: 10.1111/j.1753-318X.2009.01034.x

Fekete, A. (2009). Validation of a social vulnerability index in context to river-floods in Germany. *Natural Hazards and Earth System Science*, *9*(2), 393–403. doi: 10.5194/nhess-9-393-2009

Fielding, J., & Burningham, K. (2005). Environmental inequality and flood hazard.

Local Environment, *10*(4), 379–395. doi: 10.1080/13549830500160875

Finch, C., Emrich, C. T., & Cutter, S. L. (2010). Disaster disparities and differential recovery in New Orleans. *Population and Environment*, *31*(4), 179–202. doi: 10.1007/s11111-009-0099-8

Flanagan, B. E., Gregory, E. W., Hallisey, E. J., Heitgerd, J. L., & Lewis, B. (2011). A Social Vulnerability Index for Disaster Management. *Journal of Homeland Security and Emergency Management*, *8*(1). doi: 10.2202/1547-7355.1792

Freni, G., La Loggia, G., & Notaro, V. (2010, jun). Uncertainty in urban flood damage assessment due to urban drainage modelling and depth-damage curve estimation. *Water Science and Technology*, *61*(12), 2979–2993. doi: 10.2166/wst.2010.177

Grahn, T., & Nyberg, L. (2017). Assessment of pluvial flood exposure and vulnerability of residential areas. *International Journal of Disaster Risk Reduction*, *21*(January), 367–375. doi: 10.1016/j.ijdrr.2017.01.016

Grimm, C., Wöffler, T., Bachmann, D., & Schüttrumpf, H. (2012). Risk management in coastal engineering: Applied coastal research projects for Northern Germany. *Wasser und Abfall*, *14*, 53–55.

Hapuarachchi, H. A. P., Wang, Q. J., & Pagano, T. C. (2011). A review of advances in flash flood forecasting. *Hydrological Processes*, *2784*(March), 2771–2784. doi: 10.1002/hyp.8040

Houston, D., Werrity, A., Bassett, D., Geddes, A., Hoolachan, A., & McMillan, M. (2011). *Pluvial(rain-related) flooding in urban areas: the invisible hazard.*

Hu, L., Bao, W., Shi, P., Wang, J., & Lu, M. (2020). Simulation of overland flow considering the influence of topographic depressions. *Scientific Reports*, *10*(1), 1–14. doi: 10.1038/s41598-020-63001-y

Jenson, S. K., & Domingue, J. O. (1988). Extracting topographic structure from digital elevation data for geographic information system analysis. *Photogrammetric Engineering and Remote Sensing*, *54*(11), 1593–1600.

Johnson, M. J., Munasinghe, D., Eyelade, D., & Cohen, S. (2019). An integrated evaluation of the National Water Model(NWM)-Height above nearest drainage(HAND) flood mapping methodology. *Natural Hazards and Earth System Sciences*, *19*(11), 2405–2420. doi: 10.5194/nhess-19-2405-2019

Kaźmierczak, A., & Cavan, G. (2011). Surface water flooding risk to urban communities: Analysis of vulnerability, hazard and exposure. *Landscape and Urban Planning*, *103*(2), 185–197. doi: 10.1016/j.landurbplan.2011.07.008

Kron, W. (2005). Flood risk = hazard • values • vulnerability. *Water International*, *30*(1), 58–68. doi: 10.1080/02508060508691837

Le, P. V. V., & Kumar, P. (2014). Power law scaling of topographic depressions and their hydrologic connectivity. *Geophysical Research Letters*, *41*(5), 1553–1559. doi: 10.1002/2013GL059114

Lee, D., & Jung, J. (2014). The growth of low-income population in floodplains: A case study of Austin, TX. *KSCE Journal of Civil Engineering*, *18*(2), 683–693. doi: 10.1007/s12205-014-0205-z

Lewin, J., & Ashworth, P. J. (2014). The negative relief of large river floodplains. *Earth-Science Reviews*, *129*, 1–23. doi: 10.1016/j.earscirev.2013.10.014

Li, S., MacMillan, R. A., Lobb, D. A., McConkey, B. G., Moulin, A., & Fraser, W. R. (2011). Lidar DEM error analyses and topographic depression identification in a hummocky landscape in the prairie region of Canada. *Geomorphology*, *129*(3-4), 263–275. doi: 10.1016/j.geomorph.2011.02.020

Lindsay, J. B., & Creed, I. F. (2005). Removal of artifact depressions from digital elevation models: Towards a minimum impact approach. *Hydrological Processes*, *19*(16), 3113–3126. doi: 10.1002/hyp.5835

Luke, A., Sanders, B. F., Goodrich, K. A., Feldman, D. L., Boudreau, D., Eguiarte, A., . . . Matthew, R. A. (2018). Going beyond the flood insurance rate map: Insights from flood hazard map co-production. *Natural Hazards and Earth*

System Sciences, *18*(4), 1097–1120. doi: 10.5194/nhess-18-1097-2018

Martz, L. W., & Garbrecht, J. (1999). An outlet breaching algorithm for the treatment of closed depressions in a raster DEM. *Computers and Geosciences*, *25*(7), 835–844. doi: 10.1016/S0098-3004(99)00018-7

McCarthy, S., Tunstall, S., Parker, D., Faulkner, H., & Howe, J. (2007). Risk communication in emergency response to a simulated extreme flood. *Environmental Hazards*, *7*(3), 179–192. doi: 10.1016/j.envhaz.2007.06.003

Metz, M., Mitasova, H., & Harmon, R. S. (2011). Efficient extraction of drainage networks from massive, radar-based elevation models with least cost path search. *Hydrology and Earth System Sciences*, *15*(2), 667–678. doi: 10.5194/hess-15-667-2011

Middelmann-Fernandes, M. H. (2010). Flood damage estimation beyond stage-damage functions: An Australian example. *Journal of Flood Risk Management*, *3*(1), 88–96. doi: 10.1111/j.1753-318X.2009.01058.x

Moftakhari, H. R., AghaKouchak, A., Sanders, B. F., Allaire, M., & Matthew, R. A. (2018). What Is Nuisance Flooding? Defining and Monitoring an Emerging Challenge. *Water Resources Research*, *54*(7), 4218–4227. doi: 10.1029/2018WR022828

Muthusamy, M., Casado, M. R., Salmoral, G., Irvine, T., & Leinster, P. (2019). A remote sensing based integrated approach to quantify the impact of fluvial and pluvial flooding in an urban catchment. *Remote Sensing*, *11*(5). doi: 10.3390/rs11050577

National Academies of Sciences Engineering and Medicine. (2019). *Framing the Challenge of Urban Flooding in the United States*. Washington, D.C.: The National Academies Press. doi: https://doi.org/10.17226/25381

Nelson, K. S., Abkowitz, M. D., & Camp, J. V. (2015). A method for creating high resolution maps of social vulnerability in the context of environmental hazards. *Applied Geography*, *63*, 89–100. doi: 10.1016/j.apgeog.2015.06.011

Nobre, A. D., Cuartas, L. A., Hodnett, M., Rennó, C. D., Rodrigues, G., Silveira, A., ... Saleska, S. (2011). Height Above the Nearest Drainage - a hydrologically relevant new terrain model. *Journal of Hydrology*, *404*(1-2), 13–29. doi: 10.1016/j.jhydrol.2011.03.051

Passalacqua, P., Do Trung, T., Foufoula-Georgiou, E., Sapiro, G., & Dietrich, W. E. (2010). A geometric framework for channel network extraction from lidar: Nonlinear diffusion and geodesic paths. *Journal of Geophysical Research*, *115*(F1), 1–18. doi: 10.1029/2009jf001254

Peduzzi, P., Dao, H., Herold, C., & Mouton, F. (2009). Assessing global exposure and vulnerability towards natural hazards: The Disaster Risk Index. *Natural Hazards and Earth System Science*, *9*(4), 1149–1159. doi: 10.5194/nhess-9-1149-2009

Rolfe, M. I., Pit, S. W., McKenzie, J. W., Longman, J., Matthews, V., Bailie, R., & Morgan, G. G. (2020). Social vulnerability in a high-risk flood-affected rural region of NSW, Australia. *Natural Hazards*, *101*(3), 631–650. doi: 10.1007/s11069-020-03887-z

Rufat, S., Tate, E., Burton, C. G., & Maroof, A. S. (2015). Social vulnerability to floods: Review of case studies and implications for measurement. *International Journal of Disaster Risk Reduction*, *14*, 470–486. doi: 10.1016/j.ijdrr.2015.09.013

Rufat, S., Tate, E., Emrich, C. T., & Antolini, F. (2019). How Valid Are Social Vulnerability Models? *Annals of the American Association of Geographers*, *109*(4), 1131–1153. doi: 10.1080/24694452.2018.1535887

Sangireddy, H., Carothers, R. A., Stark, C. P., & Passalacqua, P. (2016). Controls of climate, topography, vegetation, and lithology on drainage density extracted from high resolution topography data. *Journal of Hydrology*, *537*, 271–282. doi: 10.1016/j.jhydrol.2016.02.051

Smit, B., & Wandel, J.   (2006).   Adaptation, adaptive capacity and vulnerability. *Global Environmental Change*, *16*(3), 282–292.   doi: 10.1016/j.gloenvcha.2006 .03.008

Soille, P., Vogt, J., & Colombo, R.   (2003).   Carving and adaptive drainage enforcement of grid digital elevation models. *Water Resources Research*, *39*(12), 1–13. doi: 10.1029/2002WR001879

Syvitski, J. P., Overeem, I., Brakenridge, G. R., & Hannon, M.   (2012).   Floods, floodplains, delta plains - A satellite imaging approach. *Sedimentary Geology*, *267-268*, 1–14. doi: 10.1016/j.sedgeo.2012.05.014

Tate, E., Rahman, M. A., Emrich, C. T., & Sampson, C. C. (2021). Flood exposure and social vulnerability in the United States.   *Natural Hazards*(0123456789). doi: 10.1007/s11069-020-04470-2

Tate, E., Strong, A., Kraus, T., & Xiong, H.   (2016).   Flood recovery and property acquisition in Cedar Rapids, Iowa. *Natural Hazards*, *80*(3), 2055–2079. doi: 10 .1007/s11069-015-2060-8

Teng, J., Jakeman, A. J., Vaze, J., Croke, B. F., Dutta, D., & Kim, S.   (2017). Flood inundation modelling: A review of methods, recent advances and uncertainty analysis.   *Environmental Modelling and Software*, *90*, 201–216.   doi: 10.1016/j.envsoft.2017.01.006

Tsai, C. W.   (2003).   Applicability of Kinematic, Noninertia, and Quasi-Steady Dynamic Wave Models to Unsteady Flow Routing.   *Journal of Hydraulic Engineering*, *129*(8).   doi: https://doi.org/10.1061/(ASCE)0733-9429(2003) 129:8(613)

Ueland, J., & Warf, B.   (2006).   Racialized Topographies: Altitude and Race in Southern Cities.   *Geographical Review*, *96*(1), 50–78.   doi: 10.1111/ j.1931-0846.2006.tb00387.x

UNDP.   (2010).   *Human Development Report 2010: The Real Wealth of Nations - Pathways to Human Development.* (Tech. Rep.).   New York.   doi: 10.2307/ 2137795

Wahl, T., Jain, S., Bender, J., Meyers, S. D., & Luther, M. E.   (2015).   Increasing risk of compound flooding from storm surge and rainfall for major US cities. *Nature Climate Change*, *5*(12), 1093–1097. doi: 10.1038/nclimate2736

Wing, O. E., Bates, P. D., Smith, A. M., Sampson, C. C., Johnson, K. A., Fargione, J., & Morefield, P.   (2018).   Estimates of present and future flood risk in the conterminous United States.   *Environmental Research Letters*, *13*(3).   doi: 10.1088/1748-9326/aaac65

Wing, O. E., Pinter, N., Bates, P. D., & Kousky, C.   (2020).   New insights into US flood vulnerability revealed from flood insurance big data. *Nature Communications*, *11*(1), 1–10. doi: 10.1038/s41467-020-15264-2

Winsemius, H. C., Aerts, J. C., Van Beek, L. P., Bierkens, M. F., Bouwman, A., Jongman, B., . . . Ward, P. J.   (2016).   Global drivers of future river flood risk. *Nature Climate Change*, *6*(4), 381–385. doi: 10.1038/nclimate2893

Wu, Q., Deng, C., & Chen, Z. (2016). Automated delineation of karst sinkholes from LiDAR-derived digital elevation models.   *Geomorphology*, *266*, 1–10.   doi: 10 .1016/j.geomorph.2016.05.006

Wu, Q., & Lane, C. R.   (2016).   Delineation and Quantification of Wetland Depressions in the Prairie Pothole Region of North Dakota.   *Wetlands*, *36*(2), 215–227. doi: 10.1007/s13157-015-0731-6

Zheng, X., Maidment, D. R., Tarboton, D. G., Liu, Y. Y., & Passalacqua, P. (2018). GeoFlood: Large-Scale Flood Inundation Mapping Based on High-Resolution Terrain Analysis.   *Water Resources Research*, *54*(12), 10, 013–10, 033.   doi: 10.1029/2018WR023457